Measurements and modeling of acetone laser-induced fluorescence with implications for temperature-imaging diagnostics

Mark C. Thurber, Frédéric Grisch, Brian J. Kirby, Martin Votsmeier, and Ronald K. Hanson

Recent determinations of the temperature dependence of acetone fluorescence have permitted the application of acetone planar laser-induced fluorescence imaging, which was already popular for mapping concentration, to the measurement of temperature. With a view toward developing temperature-imaging diagnostics, we present atmospheric-pressure fluorescence and absorption results acquired with excitation at eight wavelengths across the absorption feature of acetone and at temperatures from 300 to 1000 K. Modeling of the fluorescence yield of acetone is shown to be useful in explaining both these results and the variation of acetone fluorescence with pressure and composition that was observed in several studies. The model results in conjunction with the photophysics data provide guidance for the application of temperature diagnostics over a range of conditions while also suggesting useful multiparameter imaging approaches.

OCIS codes: 280.0280, 280.1740, 280.2490, 260.2510, 300.2530.

1. Introduction

Acetone (CH_3COCH_3) has found wide use as a tracer molecule in planar laser-induced fluorescence (PLIF) imaging of species concentration.[1–8] Its appeal includes low toxicity, low cost, and a high vapor pressure that permits seeding in high concentrations. A broad absorption feature (~225 to 320 nm) is accessible with high-energy, pulsed UV lasers. Fluorescence occurs between 350 and 550 nm, permitting detection with low-noise, unintensified CCD cameras.

Early applications of acetone PLIF were to turbulent free jets[1] and to jets in crossflow,[2] for which the technique was used to resolve detailed jet structure. Smith and Mungal[7] refined the jet-in-crossflow measurements, obtaining quantitative, high signal-to-noise ratio images of jet mixture fractions. In other studies acetone was employed as a marker of unburned fuel in reacting environments: methane and hydrogen jet diffusion flames,[3,5] supersonic reacting mixing layers,[3] and an internal-combustion engine.[6,8]

Quantitative interpretation of acetone signal as a function of concentration is straightforward in isothermal, isobaric flows, such as have been considered in a variety of mixing configurations. In this case, with assumption of a constant fluorescence yield, fluorescence signal is directly proportional to acetone number density. Unlike in the case of some important diatomic tracers (e.g., OH and NO), the fluorescence yield is limited by fast intersystem crossing rather than by collisional quenching, significantly reducing the composition and pressure dependences of the fluorescence yield. In the past, the assumptions of a constant fluorescence yield and an absorption cross section that is only weakly dependent on temperature were used to justify semiquantitative interpretation of acetone fluorescence images in flows with temperature variation.

In more recent studies[4,8,9] it has become apparent that acetone fluorescence does in fact have a significant temperature dependence that varies with excitation wavelength. Temperature effects were described by Tait and Greenhalgh,[4] who observed an increase in acetone fluorescence per unit absorber density with temperature for 308-nm excitation.

When this research was performed all the authors were with the High Temperature Gasdynamics Laboratory, Department of Mechanical Engineering, Stanford University, Stanford, California 94305-3032. The permanent address for F. Grisch is the Office National d'Études et de Recherches Aérospatiales, Fort de Palaiseau, 91120 Palaiseau, France.

Received 29 September 1997; revised manuscript received 31 March 1998.

0003-6935/98/214963-16$15.00/0

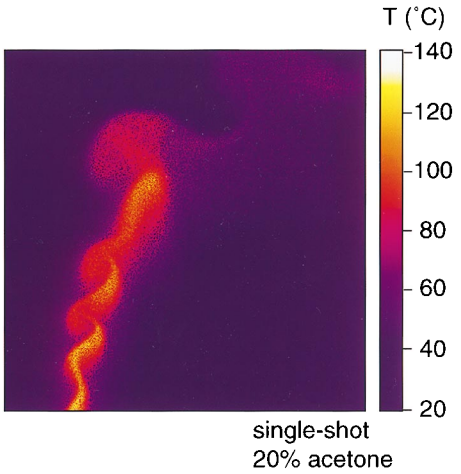

Fig. 1. Acetone PLIF temperature image obtained with 266-nm excitation and a flow field uniformly composed of 20% acetone in air. Instabilities are evident in this heated jet ($Re = 100$) in weak crossflow. The imaged region is 22 mm on a side.

Grossmann *et al.*[9] noted temperature and wavelength dependences in the fluorescence of acetone and 3-pentanone, which they attributed to a redshift in the absorption spectra with increasing temperature. Although temperature dependences complicate quantitative determination of number density from fluorescence measurements, they suggest good potential for temperature diagnostics based on knowledge of the excitation-wavelength-dependent variation of acetone fluorescence with temperature. A better understanding of temperature dependences also permits quantitative determination of number density or mole fraction from fluorescence measurements in nonisothermal flows.

Here we explore the current knowledge of acetone fluorescence photophysics as it is relevant to the application of acetone PLIF temperature diagnostics. First we present the details of experimental results that describe the wavelength-dependent variation of acetone fluorescence with temperature at atmospheric pressure.[10] In research that was reported separately,[11] these results have made possible the demonstration of single- and dual-wavelength temperature-imaging diagnostics in atmospheric-pressure flow fields. A sample temperature-imaging result (Fig. 1) is shown here to motivate consideration of acetone fluorescence dependences. In this image we see the ability of acetone PLIF to capture instantaneous temperature structure in an unstable heated jet in weak crossflow where both streams contain 20% acetone seeded into air. Laser sheet excitation at 266 nm from a frequency-quadrupled Nd:YAG laser generates an image of fluorescence, which is collected onto the CCD array of a Photometrics CH-250 unintensified camera. Based on the experimentally determined variation of acetone fluorescence with temperature for 266-nm excitation, and using a single calibration point in the flow, one can quantitatively convert fluorescence to temperature to produce the image shown.

Extension of such imaging diagnostics to other conditions will require knowledge of how the fluorescence of acetone can be expected to change with pressure and composition as well as with temperature and excitation wavelength. Such efforts are particularly important in light of recent studies[9,12,13] that have shown pressure to have a more significant effect on fluorescence than was originally believed, given the intersystem-crossing-limited nature of the fluorescence yield. Therefore our second objective in this paper is the formulation of a simple model that explains existing fluorescence data and permits extrapolation to other conditions. Following description and evaluation of an appropriate photophysical model, we explore the implications of the model for the application of diagnostics that measure temperature and other quantities over a range of conditions.

2. Temperature Dependence of Acetone Fluorescence

A. Temperature-Dependent Quantities in the Fluorescence Equation

Both the absorption and the fluorescence efficiencies of acetone depend on temperature and excitation wavelength. At room temperature and atmospheric pressure, acetone has a broadband absorption feature that extends from 225 to 320 nm,[14] with a flat peak from 270 to 280 nm; significant vibrational structure has been resolved only at low temperatures and pressures.[15,16] Fluorescence in the wavelength range from 350 to 550 nm is emitted from the first excited singlet state S_1 following laser excitation from the ground electronic state S_0.[17] Rapid intersystem crossing from S_1 to the first excited triplet T_1 limits the fluorescence yield and allows phosphorescence to occur from T_1 on a long time scale.[18] Detailed low-pressure studies[19–22] of the intersystem crossing process in acetone have revealed it to be characteristic of an intermediate-case molecule. The excited singlet evolves rapidly (in less than 5 ns) into a state of mixed singlet–triplet character in an intramolecular dephasing process. At pressures greater than 10 Torr, collisional quenching of the mixed singlet–triplet state into the triplet is rapid[19,20]; therefore the conceptual model of direct nonradiative relaxation from singlet to triplet is adequate under most conditions and is used in this paper.

Fluorescence from acetone can be modeled as shown in Eq. (1). For weak excitation the fluorescence signal, with wavelength and temperature dependences highlighted, is given by

$$S_f(\lambda, T) = \eta_{\text{opt}} \frac{E}{hc/\lambda} \, \mathrm{d}V_c n_{\text{abs}}(T) \sigma(\lambda, T) \phi(\lambda, T), \quad (1)$$

where η_{opt} is the overall efficiency of the collection optics, E is the laser fluence (J/cm^2), (hc/λ) is the energy (J) of a photon at excitation wavelength λ, and $\mathrm{d}V_c$ is the collection volume (cm^3). The temperature-dependent quantities are n_{abs}, the number density of absorbing molecules (cm^{-3}); σ, the molecular absorption cross section of the tracer (cm^2);

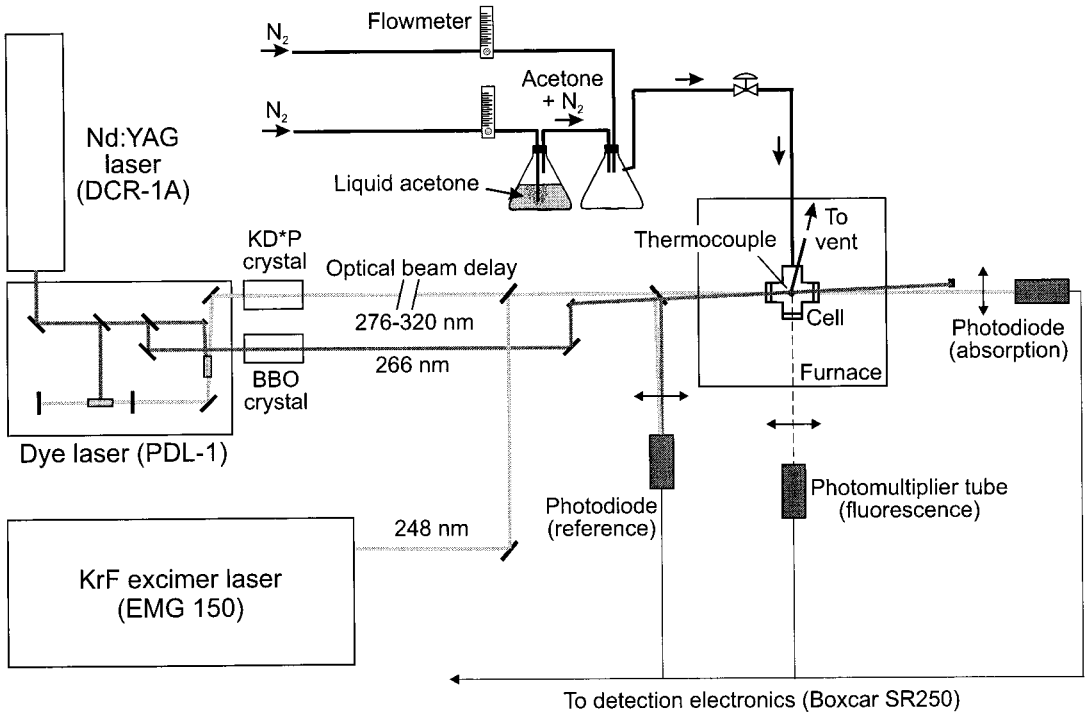

Fig. 2. Experimental schematic for acetone fluorescence and absorption temperature-dependence experiments. An acetone–nitrogen mixture is passed through a heated, optically accessible flow cell. Laser excitation is provided by a KrF excimer laser (248 nm), a frequency-quadrupled Nd:YAG laser (266 nm), and a Nd:YAG-pumped dye laser (276–320 nm).

and ϕ, the fluorescence quantum yield. Note that both σ and ϕ depend on excitation wavelength λ as well as on temperature T.

To isolate the wavelength and temperature dependences it is useful to introduce specific notation for two fluorescence quantities: S_f^* is the fluorescence signal per tracer molecule per unit laser fluence at fixed excitation wavelength, i.e.,

$$S_f^*(\lambda, T) \propto \sigma(\lambda, T)\phi(\lambda, T), \tag{2}$$

and S_f^+ is the corresponding signal per unit mole fraction, i.e.,

$$S_f^+(\lambda, T) \propto p/T\, \sigma(\lambda, T)\phi(\lambda, T), \tag{3}$$

where p is the total pressure in the gas. As indicated in relations (2) and (3), S_f^* and S_f^+ are both proportional to the absorption cross section times the fluorescence yield, so any wavelength dependence in these fluorescence quantities is attributable to the combined effects of σ and ϕ through this product.

Although knowledge of the temperature dependence of acetone absorption has remained limited until now, Grossman *et al.*[9] noted redshifts in the absorption spectra of acetone and 3-pentanone. Such shifts with temperature might be expected to change absorption cross section σ at a given excitation wavelength. Changes in the shape of the absorption feature, which result for example from statistical redistribution in absorbing energy levels, would also have an effect.

The nature of the temperature dependence of fluorescence quantum yield ϕ has also remained unclear. Early determinations of ϕ were made by Heicklen,[23] who measured a value of 0.0021 at a temperature of 40 °C and an excitation wavelength of 313 nm, and by Halpern and Ware,[24] who obtained a value of 0.0012 at room temperature and atmospheric pressure for the same excitation wavelength. Heicklen found little pressure dependence and relatively little wavelength dependence.

B. Experimental Approach

Experiments were undertaken to measure the dependence of the fluorescence signal on temperature at atmospheric pressure and temperatures from 295 to 1000 K for eight excitation wavelengths spaced across the absorption feature of acetone. Ultraviolet lasers were directed through a variable-temperature, optically accessible flow cell, allowing fluorescence and absorption to be measured on a relative basis. With normalization for the acetone number density and laser fluence, it was possible to separate the contributions of the absorption cross section and of the fluorescence quantum yield to the overall fluorescence.

As pictured in Fig. 2, we seeded acetone into a nitrogen carrier gas by bubbling nitrogen into a bath of acetone and extracting the vapor mixture at the top, which then contained the vapor pressure of acetone at the bath temperature diluted to 1 atm with nitrogen. To keep the bath temperature roughly constant and in equilibrium with the vapor above it, we flowed water at 17 °C around the outside of the

seeding flask. The bath temperature was continuously monitored to permit correction of the results for variations in acetone concentration that were due to vapor pressure changes. A second flask was used to dilute this initial acetone–nitrogen mixture with additional nitrogen, permitting variable acetone seeding to a maximum of approximately 21%.

Heating of this acetone–nitrogen flow was accomplished with a Thermolyne type 48000 furnace with the optically accessible flow cell mounted inside it. The cell was a stainless-steel cross measuring 7.5 cm end to end, with opposed sapphire windows (2-cm diameter) for laser entry and exit, a third sapphire window for fluorescence detection, and flow entry through the remaining arm of the cross. A type K thermocouple sealed into the cell provided real-time indication of the gas temperature at the measurement volume. Flow exited through the top of the cell. Furnace, cell, and flow were allowed a number of minutes to stabilize at each temperature before measurements were made.

Laser excitation at 248 nm was provided by a Lambda Physik EMG 150 excimer laser with a KrF mixture; wavelengths from 266 to 320 nm were generated with a Nd:YAG–dye-laser combination (Quanta Ray DCR-1A Nd:YAG pumping a Quanta-Ray PDL-1 dye laser; Fig. 2). We produced the 266-nm excitation by splitting off and directly frequency doubling a portion of the 532-nm dye-laser pump beam, whereas beams at 276, 282, 289, 300, 308, and 320 nm were formed from the frequency-doubled dye-laser output. The UV linewidths (FWHM) were of the order of 0.4 cm^{-1} for the 266–320 nm wavelengths and 50 cm^{-1} for 248 nm. For all experiments, data were collected with laser repetition rates of 10 Hz.

A flexible beam delivery system allowed for simultaneous fluorescence measurements with one beam at 248 or 266 nm and another at 276–320 nm. As shown in Fig. 2, we produced this laser excitation by splitting off a portion of the dye-laser pump beam to form a 266-nm beam for use in conjunction with the dye-laser output or by synchronizing the UV pulses from the dye laser to the KrF excimer at 248 nm. In both cases the respective beams, separated in time by ~100 ns, were brought into the cell at a slight angle (<0.7°) to each other, intersecting at the center of the cell. Both were approximately 3 mm in diameter, with comparable energies of ~0.6 mJ/pulse for the fluorescence experiments. Laser energies were registered for each pulse by two gated integrator–boxcar averager modules (Stanford Research Systems SR250), separately gated around each of the two pulses measured by a fast photodiode collecting a split-off portion of the incident beams. Two more boxcars, with 90-ns gate widths, allowed a single photomultiplier tube to collect the fluorescence that was due to both excitation pulses, thereby ensuring identical collection optics for the two cases. All fluorescence measurements were normalized by the recorded laser energies. Rejection of stray laser light was provided by the sharp drop-off in the response of the Hamamatsu 1P21 photomultiplier tube below 300 nm. Additional attenuation in the ultraviolet was achieved by a 2-mm-thick Schott WG305 filter, while a 2-mm BG28 filter reduced radiation above 550 nm. To stay in the optically thin regime for the fluorescence measurements we seeded acetone into the nitrogen carrier gas at the comparatively low mole fraction of 7500 parts in 10^6 for the fluorescence experiments. Flow velocities in the feed line were typically ~19 m/s, resulting in a furnace residence time (time between when the gas enters the furnace and when it passes through the measurement volume), τ_{res}, of approximately 0.1 s.

Each measurement of absorption cross section employed only a single incident beam, with a second photodiode mounted after the furnace to measure the energy of the laser after it had passed through the cell. Fractional transmission measurements, combined with knowledge of the acetone number density from the flow rates and the acetone bath temperature, allowed absorption cross-sections to be determined from Beer's law. Transmission through the cell with acetone flowing at a particular rate was divided by transmission without acetone to remove the effect of losses through the cell windows. To increase the sensitivity of the absorption measurements we introduced acetone in the highest possible concentration of ~21% by eliminating the second nitrogen dilution stage. The lower flow rates employed in the absorption experiments resulted in furnace residence times of 0.3–2 s. The gas was estimated to be in the cell for 0.7 s at the lowest flow rate and for 0.1 s at the highest flow rate.

Before the experimental measurements, the linearity of fluorescence with both laser fluence and acetone concentration was verified at the two ends of the temperature range for all the wavelengths considered. In keeping with the pyrolysis time constants of Ernst *et al.*,[25] pyrolysis did not appear to be an issue in the fluorescence measurements for the residence time (τ_{res} ~ 0.1 s) and temperature range considered. This conclusion was supported by absorption coefficient measurements at temperatures as high as 900 K, in which the results did not change as furnace residence time was decreased to 0.3 s and less.

Experiments showed relatively little effect of temperature on the shape and position of the fluorescence spectrum, indicating that use of an optical collection system with different spectral transmission characteristics is unlikely to change significantly the measured relative dependence of fluorescence on temperature. For 266-nm excitation, experiments suggested perhaps a 5–15-nm shift of the fluorescence feature to the blue at the high temperature, whereas for 308-nm excitation there appeared to be a 10–20-nm shift to the blue.

C. Results: Temperature and Wavelength Dependences

Fluorescence results are presented in two ways: first, on a per-density or per-mole basis (S_f^*; Fig. 3) to permit a general examination of the fluorescence behavior

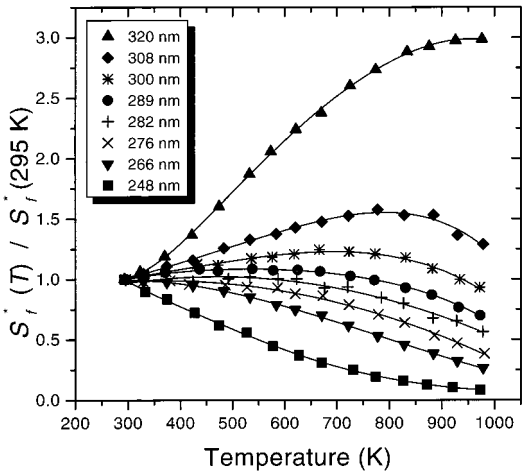

Fig. 3. Fluorescence per molecule per unit laser fluence at atmospheric pressure, normalized to the room-temperature value for each wavelength and plotted as a function of temperature for all eight excitation wavelengths. For this figure and subsequent figures in this section, symbols represent experimental data points and lines are fits to the data. Error is estimated to be ±2% at low temperatures and from ±3 to ±4% at higher temperatures.

and its sources, and later on a per-mole-fraction basis (S_f^+; Fig. 7 below) and as signal ratios (Fig. 8 below), for the purposes of evaluating diagnostic strategies. Combining the fluorescence and absorption data sets permits consideration of the separate contributions of absorption cross section σ (Figs. 4 and 5) and fluorescence quantum yield ϕ (Fig. 6, generated by division of the fluorescence signal by the absorption cross section) to the overall fluorescence.

The fluorescence-per-absorber-density results given in Fig. 3, in which each curve has been normalized to the room-temperature fluorescence value, show a continuous transition from a steady increase with temperature at 320 nm to a steady decrease at

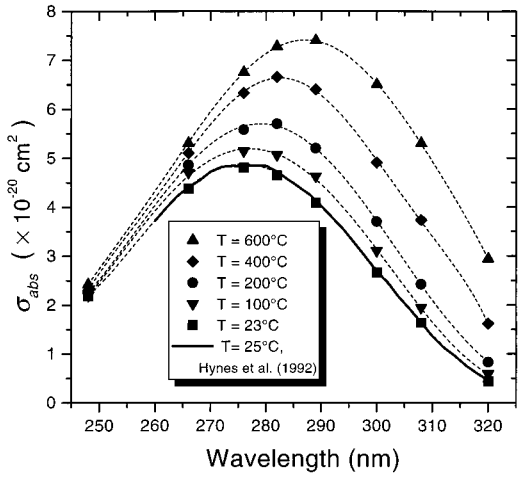

Fig. 4. The absorption spectral profile of acetone is seen both to shift to longer wavelengths and to increase in magnitude as temperature is increased. Error in the absorption measurements is typically ±2–±3%. Room-temperature data from this study match the results of Hynes *et al.*[14]

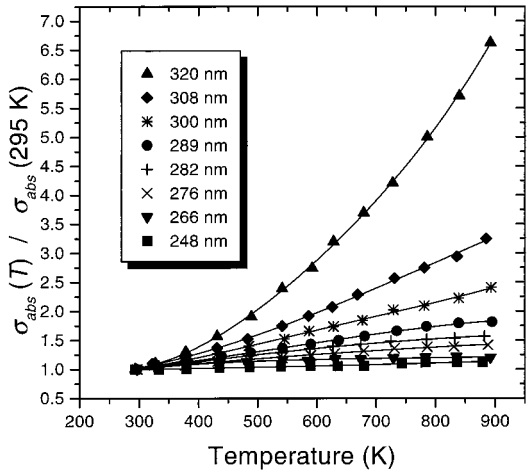

Fig. 5. The normalized absorption cross section of acetone shows a steady rise with temperature, with the effect increasing with wavelength. Eight excitation wavelengths are plotted.

248 nm. The results are in qualitative agreement with the limited fluorescence data previously reported, increasing from 300 to 700 K for 308 nm, in rough correspondence with the results of Tait and Greenhalgh,[4] and decreasing with 266-nm excitation from 300 to 600 K, although not so much as indicated by Ghandhi and Felton.[8] Each data point in Fig. 3 is the average of 300 measurements for all wavelengths except 308 nm (900 measurements) and 266 nm (1800 measurements). In this figure, as in the other figures in this section, curves represent fits to the data. Experimental error is estimated to be ±2% at low temperatures and from ±3 to ±4% at higher temperatures.

The temperature and wavelength dependences of the fluorescence per absorber density arise from the product of absorption cross section and fluorescence yield. The room-temperature absorption feature shown in Fig. 4 matches that recorded by Hynes *et*

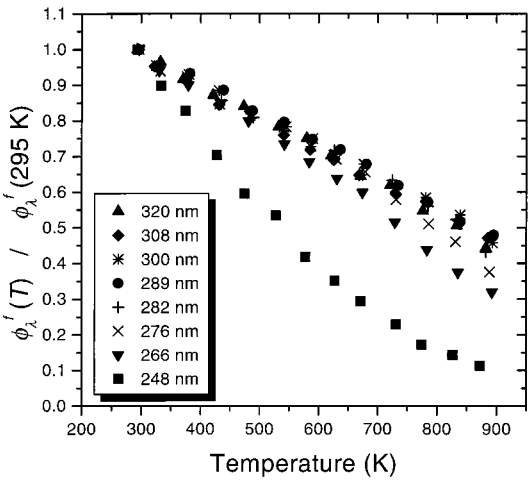

Fig. 6. Relative temperature dependence of the fluorescence yield, obtained by division of the normalized fluorescence signal by the normalized absorption cross section at each temperature.

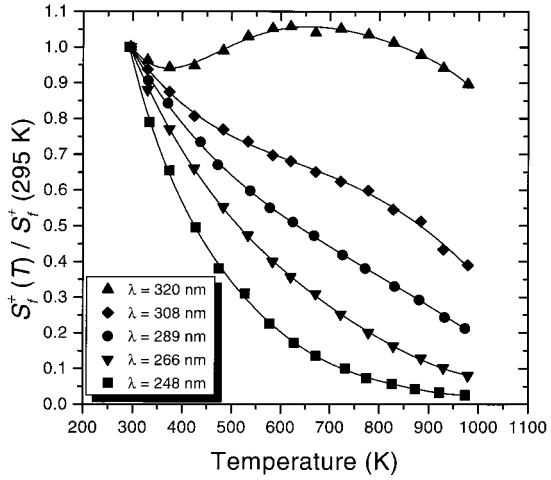

Fig. 7. Fluorescence per unit laser energy per unit mole fraction at atmospheric pressure, normalized to the room-temperature value. At constant pressure and seeding fraction, temperature can be inferred from a fluorescence measurement with this plot. For clarity, only five excitation wavelengths are considered.

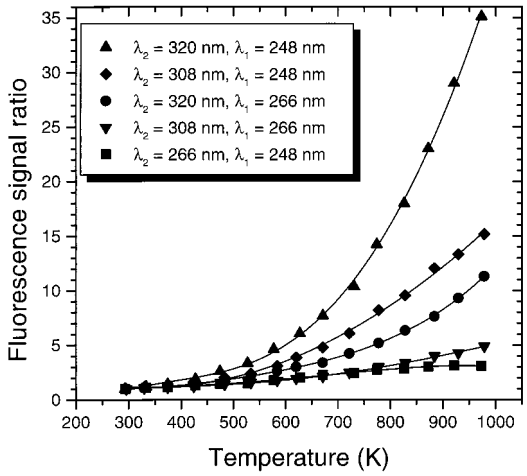

Fig. 8. Fluorescence signal ratios (P = 1 atm) produced by five different wavelength combinations, plotted as a function of temperature. Each data point represents the ratio of the longer-wavelength fluorescence signal at a given temperature to the shorter-wavelength signal at the same temperature.

al.[14] As temperature is increased, the absorption spectral profile increases in magnitude and width and shifts towards the red. As Fig. 5 shows, the absorption cross section increases with increasing temperature for all wavelengths considered, changing only slightly with temperature at the shorter wavelengths and significantly at the longer ones. Errors in the absorption measurements are typically ±2–±3%.

The relative behavior of fluorescence yield ϕ, generated by division of the fluorescence data of Fig. 3 by the absorption data of Fig. 5, is pictured in Fig. 6. For all wavelengths, the fluorescence yield decreases with increasing temperature. The decrease appears to be somewhat steeper at shorter wavelengths.

D. Diagnostic Strategies

Leaving aside for the moment possible effects of pressure and composition as one moves away from the 1-atm condition at which the data in this study were acquired, we can use the present fluorescence results to evaluate candidate strategies for temperature diagnostics. For measurements of concentration (density or mole fraction), Figs. 3 and 7 can aid in the selection of excitation wavelengths that result in minimal temperature dependence. From Fig. 3, excitation near 289 nm appears optimal for low-temperature species density measurements. Figure 7, in which fluorescence per unit mole fraction is plotted with temperature, suggests that longer wavelengths are best for mole fraction measurements with the least temperature dependence.

For measurements of temperature, on the other hand, there are at least two promising strategies (demonstrated and discussed in greater detail separately[11]) that can be evaluated by use of Figs. 7 and 8. In cases with constant pressure and a uniform seeding of acetone (i.e., a fixed but possibly unknown mole fraction), relation (3) indicates that temperature can be inferred directly from a single-wavelength fluorescence measurement by application of the curve in Fig. 7 for the excitation wavelength of choice. Both 248 and 266 nm are seen to be attractive excitation wavelengths, with steep changes in fluorescence with temperature. An alternative approach to temperature measurement is to use two excitation wavelengths, with the laser pulses slightly separated in time and the images recorded separately. In this case temperature is inferred from the ratio of measured fluorescence signals, which is a single-valued function of temperature, as can be seen from Fig. 8. Acetone density at a given point in the flow cancels in this ratio. Although it is more complex and demanding in equipment, this dual-wavelength approach is useful for flows that lack uniform acetone concentration. Figure 8, which plots some fluorescence ratios with temperature, shows short-wavelength–long-wavelength pairs to be ideal. Experimentally, 308–248 nm and 308–266 nm are attractive wavelengths because they are accessible with high-energy, pulsed UV lasers.

3. Photophysics Modeling

A. Background and Motivation

The demonstrated potential of acetone temperature imaging at atmospheric pressure[11] provides motivation for applications at other conditions. Modeling, in particular of the pressure and composition effects on fluorescence that arise through the fluorescence quantum-yield term, can allow the 1-atm acetone–nitrogen data of Figs. 7 and 8 to be extended to other regimes for wider diagnostic application. Modeling efforts also suggest which diagnostic strategies for measuring temperature and other parameters will be optimal at given conditions. Finally, development of a model consistent with observed fluorescence variation with temperature, pressure, composition, and

excitation wavelength lends insight into the photophysical behavior of the acetone molecule.

The early work of Heicklen[23] suggested that pressure dependences of acetone fluorescence were minimal, and this finding seemed to be in keeping with the fact that acetone has a rapid intersystem crossing. However, recent studies[9,12,13] have elucidated pressure and composition dependences that, although they are often weaker than those that are due to temperature at a given excitation wavelength, are nonetheless significant enough that they need to be considered when one is designing diagnostic strategies. Two main observations seem to be common to these studies: fluorescence intensity per molecule increases with pressure (except in some cases at high pressure) and the presence of oxygen appears to reduce the fluorescence intensity in a way that becomes significant above 3–5 atm.

B. Simple Conceptual Model

An increase in pressure can be consistent with an increase in fluorescence yield if the nonradiative electronic relaxation rate k_{NR} (here considered equal to the intersystem crossing rate k_{ISC}) that limits the fluorescence efficiency is an increasing function of vibrationally excited level in the excited singlet state. Such a k_{NR} functionality is indeed observed in other hydrocarbons.[26,27] As pressure increases in such a case, collisional vibrational relaxation will more rapidly return molecules from high-lying, initially excited singlet states to less energetic vibrational states. Because the intersystem crossing is slower from these lower-lying levels, the fluorescence yield will be higher. In this way, competition between intersystem crossing and vibrational relaxation in the excited singlet manifold modifies the fluorescence yield. Yuen *et al.*[12] put forward this conceptual model to explain their results for the pressure dependence of acetone fluorescence.

This model is also consistent with the observed temperature dependences of the fluorescence yield (Fig. 6). As temperature is increased, an acetone molecule in the ground singlet state will on average have more vibrational energy. It will therefore be pumped into an initial state higher above the S_1 origin[15] ($\sim$30,440 cm^{-1}) and will thermalize to a higher vibrational state in the excited singlet. Assuming that intersystem crossing rates increase with energy above the origin, this higher-temperature molecule will, on average, cross to the triplet more efficiently, reducing the fluorescence yield.

The trend in fluorescence yield with changes in excitation wavelength is also predicted by this conceptual framework. A decrease in excitation wavelength (increase in excitation energy) will place the molecule in a higher initial level of the excited singlet, exposing it to higher intersystem crossing rates and therefore decreasing the fluorescence yield. Such a drop in fluorescence yield with decreasing excitation wavelength was observed experimentally by Shortridge *et al.*,[28] who showed a roughly linear variation of the fluorescence yield with wavelength over most of the range from 260 to 320 nm.

C. Quantitative Model: Multistep Decay

A multistep decay model can incorporate these observations about the behavior of the fluorescence yield into a quantitative framework, permitting comparison with data and extrapolation to other conditions. Wilson *et al.*[29] used a multistep decay formulation to consider the pressure dependence of fluorescence spectra. Analogous multistep deactivation models have also been widely applied by others[30–33] to study collisional deactivation in photochemical dissociation reactions.

The specific multistep decay model that we use here is pictured schematically in Fig. 9. The fluorescence decay of an average molecule is considered. This molecule initially sits in thermal equilibrium at some energy $\Delta E_{thermal}(T)$ above the $v'' = 0$ level of the ground singlet state S_0. It is excited by a laser, which pumps it with an energy ΔE_{laser} to the excited singlet state S_1. The combination of the initial thermal energy and the laser excitation energy determines the molecule's initial energy E above the excited singlet origin. The molecule decays in E because of discrete collisional events. From each vibrationally excited level that it occupies in the S_1 manifold, the molecule can nonradiatively decay through intersystem crossing, with a rate $k_{NR}(E)$; fluoresce back to S_0, with a rate k_f; or decay to a lower vibrational level in S_1, with a rate equal to a collision rate $k_{coll}(T, P)$. Eventually the molecule reaches the thermalized level, $\Delta E_{thermal}(T)$, above the origin, from which it can either cross to the triplet or fluoresce back to the ground singlet. Note that, although the nonradiative electronic relaxation of the excited singlet is assumed to be due to intersystem crossing, it could equally well be due to any combination of intramolecular processes (including internal conversion or predissociation, for example) for the purpose of the model.

To determine the fluorescence yield ϕ, the model sums over all the N vibrational levels in the excited singlet occupied by this average molecule as it decays [Eq. (4)], with level 1 being the initially excited state and level N a state sufficiently close to the thermalized level, at which the summation is terminated:

$$\phi = \frac{k_f}{k_f + k_{coll} + k_{NR,1}} + \sum_{i=2}^{N-1} \left(\frac{k_f}{k_f + k_{coll} + k_{NR,i}} \prod_{j=1}^{i-1} \left[\frac{k_{coll}}{k_f + k_{coll} + k_{NR,j}} \right] \right) + \frac{k_f}{k_f + k_{NR,N}} \prod_{j=1}^{N-1} \left[\frac{k_{coll}}{k_f + k_{coll} + k_{NR,j}} \right]. \quad (4)$$

For a given vibrational level E, the contribution to the total fluorescence yield is given by the effective fluorescence yield from that level, i.e., the probability that it will fluoresce from that level rather than decaying in some other way, times the probability that

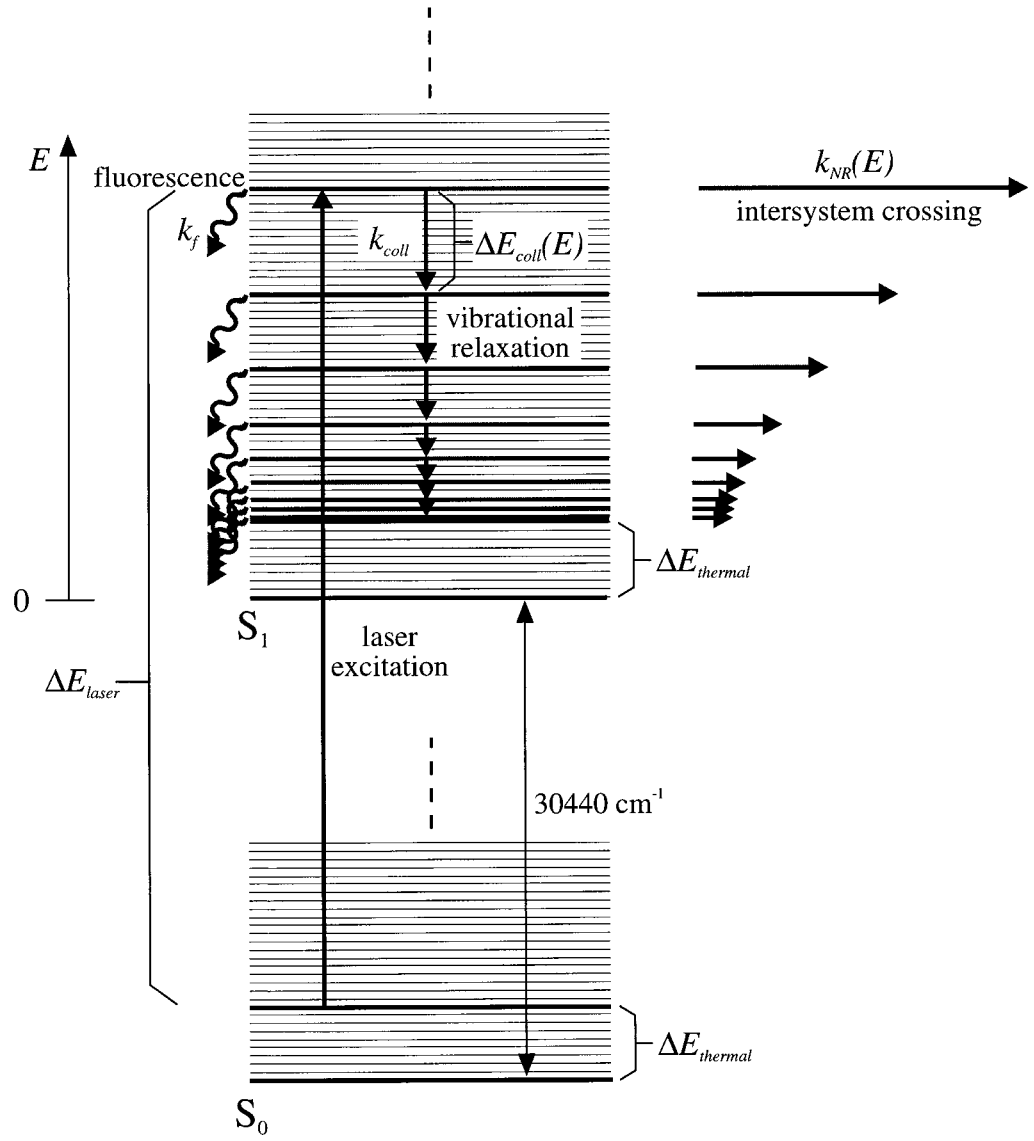

Fig. 9. Simplified model of acetone's photophysical behavior with multistep decay of the excited singlet.

the molecule will decay to that level before fluorescing or undergoing intersystem crossing. In Eq. (4) the first term is the contribution from the initially excited state, the last term is the contribution from the thermalized level, and the summation represents the contributions from the levels in between. The average energy transferred per collision, $\Delta E_{\text{coll}}(E)$, determines the energy separation of the vibrational levels through which the molecule cascades.

Model parameters must be set to allow the fluorescence yield to be predicted as a function of temperature, pressure, and excitation wavelength. The fluorescence rate k_f is assumed constant with vibrational energy E, which Lee and Lewis[34] suggest is approximately true for most carbonyl compounds. The intersystem crossing behavior is set in accord with previous results from which the rate can be extracted as a function of excess energy. The collisional model, suggested by the results of Hippler *et al.*,[35] is that the average energy transferred per collision, ΔE_{coll}, is linearly proportional to the excess energy above the thermalized level, $E - E_T$, with α defined here to be the constant of proportionality. Finally, we calculate $\Delta E_{\text{thermal}}$ as a function of T, assuming harmonic oscillators for each of the 24 vibrational modes and using the vibrational frequency data of Shimanouchi.[36]

D. Model Assumptions

Given the sparse and scattered data available, the model aims to maintain conceptual and computational simplicity while capturing the important photophysical processes involved. Three decay processes for excited singlet molecules are included: fluorescence, intramolecular electronic relaxation (primarily intersystem crossing, although dissociation[37] and internal conversion[27] could contribute at higher excitation energies), and vibrational relaxation through collisions. Collisional electronic relaxation through direct quenching from S_1 to S_0 is not considered, as

rates of electronic quenching of the singlet state are typically significantly lower than intersystem crossing rates.[17] The intersystem crossing is assumed to be irreversible and intramolecular for all practical purposes, consistent with the single-exponential decay exhibited by acetone fluorescence for the range of pressure considered.[34]

The model makes a fundamental simplification by treating the transitions of a single average molecule rather than the distribution of molecules that actually exists. This approach neglects the second-order effect of how the energy dependence of the absorption cross section distorts the upper-level energy distribution from its ground-state form, changing the average initial energy in the excited singlet state. Excited singlet energy values are treated as continuous in the model, given the dense level spacings and the broad distributions of excited molecules at the temperatures considered. The true ensemble of upward and downward collisions that maintain energy distributions are approximated by a simple downward cascade to the equilibrium level that occurs in discrete energy steps of $\Delta E_{\mathrm{coll}}(E)$.

E. Model Results and Sensitivity

The model was applied in an effort to explain the various photophysical results observed for acetone. These results include published data from which radiationless electronic relaxation rates can be extracted as a function of excited singlet energy E,[13,28,38] published data describing the pressure dependence of acetone fluorescence,[12,13] and the fluorescence-yield temperature-dependence data presented above in this paper. Pressure data sets for gas mixtures that include oxygen are not for the moment considered in model comparisons because of possible unique effects of oxygen at high pressure.

Comparison of model results with data (Figs. 10–13) shows that the model can in fact self-consistently match the available data well. The variable model parameters were $k_{\mathrm{NR}}(E)$ and the collisional energy transfer proportionality constant α. We set these parameters by using a global optimization, which sought the best match to available data for $k_{\mathrm{NR}}(E)$ and the pressure and temperature dependences of ϕ. Table 1 shows, first, the set of parameters produced by the optimization, which are employed for subsequent predictions with the model, and second, two other sets of parameters slightly off the optimum, to permit qualitative consideration of sensitivity to α. In one case, the energy transfer proportionality constant α was forced to be a factor of 3 lower than the optimized result; in the other case it was set a factor of 3 higher. In both cases the remaining parameters are optimized for the specified α. One conclusion that emerges from consideration of these two slightly off-optimum data sets is that acceptable fits to the sparse acetone fluorescence-yield data can be achieved with parameter sets that vary somewhat. As a result, the model parameters used should not at this point be taken to imply values of specific physical quantities. However, the fact that the model can self-consistently match experimental results with reasonable model parameters supports the basic soundness of the model.

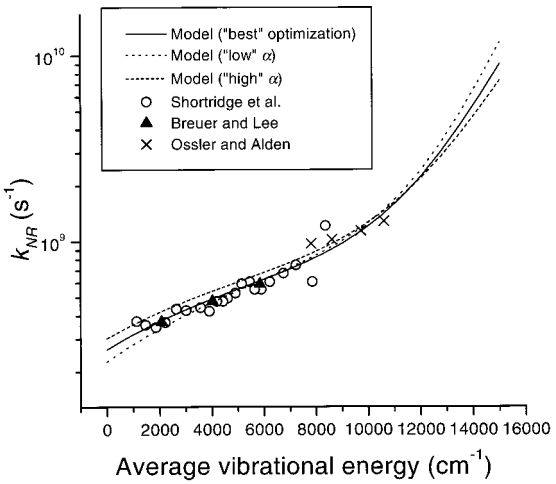

Fig. 10. Optimized model expression for k_{NR} as a function of average vibrational energy (solid curve) compared with existing data. Two slightly off-optimum model cases are also plotted (dashed and dotted curves). Low-pressure data on fluorescence lifetime (Breuer and Lee,[38] Ossler and Aldén[13]) and fluorescence yield (Shortridge *et al.*[28]) have been converted into data for $k_{\mathrm{NR}}(E)$, the electronic relaxation rate as a function of vibrational energy, under the assumption of a constant fluorescence rate k_f. Biexponential behavior of k_{NR} was assumed in the model (see Table 1).

As shown in Fig. 10, the model tracks $k_{\mathrm{NR}}(E)$ data inferred from three sources. A biexponential expression for $k_{\mathrm{NR}}(E)$ was chosen for use with the model. The first two sources of comparison data, the studies of Breuer and Lee[38] and Ossler and Aldén,[13] provide low-pressure fluorescence lifetime data for acetone. Based on the premise that the intersystem crossing rate limits the fluorescence lifetime, and on

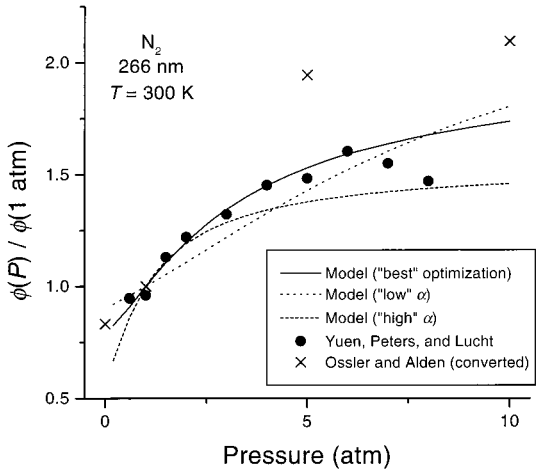

Fig. 11. Fluorescence-yield pressure-dependence data of Yuen *et al.*[12] and Ossler and Aldén[13] (converted from fluorescence lifetime data under the assumption of a constant fluorescence rate k_f) compared with the optimized model results and with slightly off-optimum model results (dotted and dashed curves).

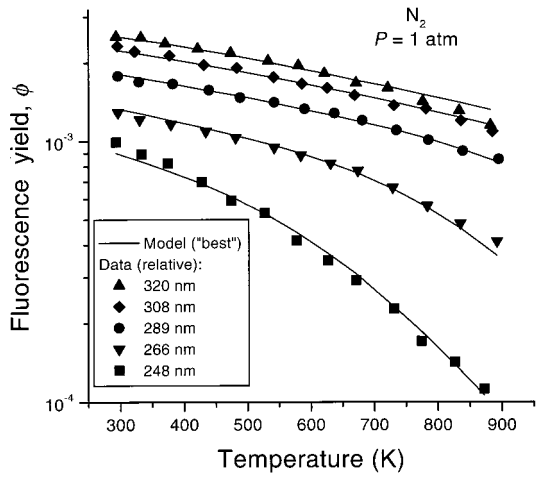

Fig. 12. Variation of the fluorescence yield with temperature and excitation wavelength plotted for the optimized model parameters on an absolute basis, with the Heicklen result at 40 °C and 313 nm as a reference. For each wavelength the temperature-dependent data reported here are compared against the model, with a constant factor (determined by best fit) used to normalize the experimental data, which carry only relative information, at each wavelength.

the additional assumption that there will be no significant vibrational relaxation on the relevant time scales at low pressure, the fluorescence lifetime can be taken as the inverse of k_{NR}. Furthermore, because there was assumed to be no relaxation, these values are, on an averaged basis, state specific to the initially pumped level in the excited singlet. The final data set, from Shortridge *et al.*,[28] plots relative fluorescence yield as a function of excitation wavelength at room temperature and low pressure. Normalizing to the value of 0.0021 for ϕ reported by Heicklen[23] at 313 nm and 40 °C, and using the fluorescence rate $k_f = 8 \times 10^5$ s found by Hansen and Lee,[18] we can convert these data into k_{NR} plotted against E. It can be seen that there are few k_{NR} data above 11 000 cm^{-1}.

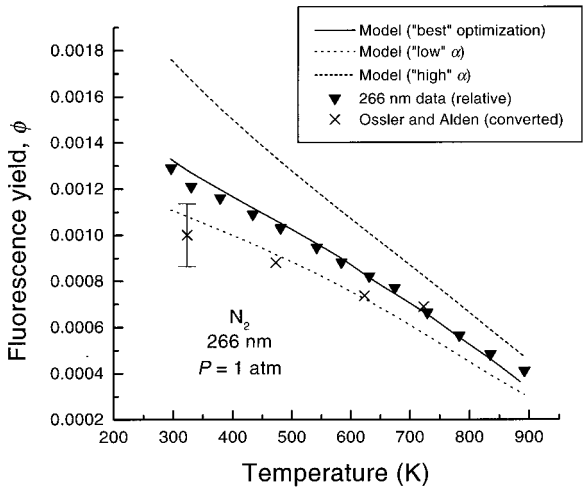

Fig. 13. Variation of fluorescence yield with temperature examined more closely for 266-nm excitation. The optimized model results and the slightly off-optimum results (dashed and dotted curves) are plotted on an absolute basis. Our relative fluorescence yield data are multiplied by a constant to provide the best fit to the model. Ossler–Aldén data are converted to fluorescence yield based on the value of fluorescence rate found by Hansen and Lee.[18]

The optimization aimed to match the intermediate pressure region (0.6–5 atm) of the fluorescence per molecule data of Yuen *et al.*[12] for 266-nm excitation and a nitrogen bath gas at room temperature. Assuming that the absorption is independent of pressure, this behavior represents the variation of the fluorescence yield. These data were chosen to be included in the optimization because they provide the most comprehensive pressure-dependence information in the intermediate-pressure regime for a nitrogen bath gas and should therefore be most sensitive to the collisional energy transfer proportionality constant α. As is apparent from Fig. 11, the optimized model is able to match this intermediate-pressure regime well, although the data points of Yuen *et al.* fall below the model at higher pressures. The data of Ossler and Aldén[13] (obtained at the slightly higher temperature of 323 K) fall somewhat above the model. The model will converge on a low-pressure limit corresponding to no vibrational relaxation and on a high-pressure limit corresponding to complete vibrational relaxation before intersystem crossing.

Figure 12 shows that the model reproduces quite well the temperature and wavelength dependences of the fluorescence yield at atmospheric pressure. The model is pinned at 313 nm and 40 °C to the Heicklen result, so it yields absolute fluorescence-yield predictions (solid curves). (Note that there is a significant uncertainty in the Heicklen value for ϕ. However, comparisons and results are kept internally consistent by use of this value for all model calculations and all conversions of published data.) The temperature-dependence data, on the other hand, were acquired only on a relative basis and are therefore normalized at each wavelength by a constant factor to best fit the corresponding model curve. The greater variation of fluorescence yield with temperature at shorter wavelengths is faithfully reproduced by the optimized model.

A more-detailed plot of fluorescence yield versus temperature for 266-nm excitation is given in Fig. 13. Our relative fluorescence yield data are normalized to fall upon the best-fit model curve. Also plotted is the absolute fluorescence-yield information inferred from multiplying the Ossler–Aldén[13] fluorescence lifetime data at 1 atm by the fluorescence rate from Hansen and Lee.[18] These data points fall closer to the low-α model curve and suggest a less steep decrease in fluorescence yield with temperature than observed in our data or model curves.

Overall, it is apparent that a good match to data can be achieved with the model and that values of the model parameters can be varied somewhat and still produce reasonable agreement. For instance, changing the collisional parameter α (or, equiva-

Table 1. Model Parameters

Parameter	Value
Best fit	
k_f (s^{-1})[a]	8×10^5
$k_{coll,\ T = 300\ K,\ P = 1\ atm}$ (s^{-1})	1.1×10^{10}
$k_{NR}(E)$ (s^{-1})	$-3.82 \times 10^9 + 8.82 \times 10^5 \exp(E/1650) + 4.08 \times 10^9 \exp(E/77300)$
α	0.021
Low-α case	
k_f (s^{-1})	8×10^5
$k_{coll,\ T = 300\ K,\ P = 1\ atm}$ (s^{-1})	1.1×10^{10}
$k_{NR}(E)$ (s^{-1})	$-6.51 \times 10^8 + 2.75 \times 10^5 \exp(E/1425) + 8.77 \times 10^8 \exp(E/16660)$
α	0.007
High-α case	
k_f (s^{-1})	8×10^5
$k_{coll,\ T = 300\ K,\ P = 1\ atm}$ (s^{-1})	1.1×10^{10}
$k_{NR}(E)$ (s^{-1})	$-2.88 \times 10^{10} + 1.73 \times 10^6 \exp(E/1833) + 2.91 \times 10^{10} \exp(E/525000)$
α	0.063

[a]Ref. 18.

lently, the collision rate k_{coll}) by a factor of 2 and then reoptimizing the other parameters results in a model that still acceptably matches the limited data for acetone fluorescence yield. However, Figs. 10, 11, and 13 imply that altering this value by a factor of 3 or more begins to affect the fit to data negatively in a significant way. These results suggest that existing photophysics data are insufficient to validate the model in a fully quantitative way and that physical parameters cannot yet be inferred from optimized model parameters. However, the basic success of the model in reconciling existing data suggests that it does capture the important photophysical processes in acetone fluorescence and that it is therefore reasonable to use the model to draw conclusions about how diagnostics for temperature and other quantities can most effectively be applied across a range of conditions.

4. Implications for Diagnostics

A. Introduction

The model that has been described allows effects of pressure and composition, as well as of temperature and excitation wavelength, to be included in the evaluation of diagnostic strategies. Pressure and composition affect fluorescence yield indirectly, modifying the vibrational relaxation rate of acetone molecules in the excited singlet state and thereby changing the distribution of vibrational levels from which fluorescence occurs. The dependence on pressure and composition is much weaker than for diatomic tracers with direct collisional quenching of the excited state but is nevertheless strong enough to be of potential importance for diagnostic applications. In the model, pressure and composition effects on fluorescence yield arise in the same way, through the energy decay rate $k_{coll}\Delta E_{coll}$, where $\Delta E_{coll} = \alpha(E - E_T)$. Collision rate k_{coll} is directly proportional to pressure; changes in composition can affect both the collision rate and the energy transfer proportionality constant α.

Pressure effects are more easily treated than composition effects because of the lack of information on collisional energy transfer in vibrationally excited acetone. Through changes in the fluorescence yield, changes in pressure will modify the fluorescence–temperature curves required for application of temperature diagnostics. By accounting for this effect, model-generated curves should provide more-accurate diagnostic results for uniform pressure applications away from 1 atm. In the single-wavelength case, application in flows with nonuniform pressure is not practical because of the direct pressure proportionality in the number density term. In the dual-wavelength case, for which the only pressure dependence is in the ratio of fluorescence yields, the model allows the feasibility of temperature diagnostics in variable pressure environments to be evaluated. To the extent that collisional properties are known, the effects of composition can be examined analogously to the effects of pressure.

In this section we use the photophysics model in conjunction with the 1-atm fluorescence–temperature data to evaluate diagnostic applications across a matrix of temperature, pressure, and excitation wavelength conditions for a fixed composition of dilute acetone in nitrogen. Frequently these results are applicable as well for other compositions, for example, acetone in air; we discuss when the effects of different or variable compositions or both cannot be neglected. Finally, we propose new multiparameter imaging strategies that are made possible by increased knowledge of acetone photophysics, and we evaluate these strategies by using the fluorescence data and the photophysical model.

B. Estimating Temperature Sensitivity and Error

Applying the data and the model to hypothetical experimental conditions allows the sensitivity of single-

and dual-wavelength temperature diagnostic strategies to be estimated across a range of conditions of temperature and pressure. Random temperature uncertainties are calculated assuming an idealized, shot-noise-limited experiment and neglecting any possible error in the fluorescence–temperature curves. For best temperature sensitivity, excitation sources are assumed to be high-pulse-energy lasers: a KrF excimer laser delivering 300 mJ of energy at 248 nm, a frequency-quadrupled Nd:YAG laser providing 100 mJ at 266 nm, and a XeCl excimer laser emitting 200 mJ at 308 nm. A 3-cm-high laser sheet passing through a nitrogen flow with acetone seeded to a partial pressure of 19 Torr is considered. The fluorescence is assumed to be imaged with $f/1.8$, 30%-efficient collection optics at 1:2 magnification onto a 512×512 pixel CCD array that has a 40% quantum efficiency.

In a dual-wavelength diagnostic with varying pressure, a critical factor in addition to sensitivity is the amount of error that will arise in the temperature measurement as the result of a change in pressure. This error can be estimated by use of the atmospheric-pressure fluorescence ratio curves of Fig. 8 along with model-generated results for the variation of fluorescence yield with pressure.

C. Single-Wavelength Temperature Imaging

Single-wavelength temperature imaging is possible for conditions of uniform pressure and acetone seeding. Figure 14 plots the model-generated normalized curves of fluorescence per laser fluence per mole fraction with temperature that would be used for single-wavelength applications at four specific pressures. The specific changes in the slopes of the curves in moving from 0.1 to 10 atm are related to the shift between low-pressure and high-pressure limiting behavior and to the fact that a change in temperature has the greatest effect on the distribution of fluorescence from different vibrational levels at intermediate pressures, near 2–3 atm.

Good sensitivity to temperature across the range of temperatures and pressures considered makes 248 and 266 nm the excitation wavelengths that are best suited for temperature diagnostics. Figure 15 shows sensitivity in a plot of families of curves of estimated random temperature uncertainty at different pressures, increasing in 0.5-atm increments from 0.5 to 5 atm. At room temperature and atmospheric pressure, temperature uncertainty as low as 0.4% (1.2 K) is indicated for 248-nm excitation. The trend of improved sensitivity with increasing pressure is due to the combination of two effects: the overall decrease in experimental uncertainty associated with the increase in signal as fluorescence yield rises and the change in the shape of the fluorescence–temperature curve. For all pressures, 248-nm sensitivity is better at lower temperatures, whereas 266-nm sensitivity is better at higher temperatures.

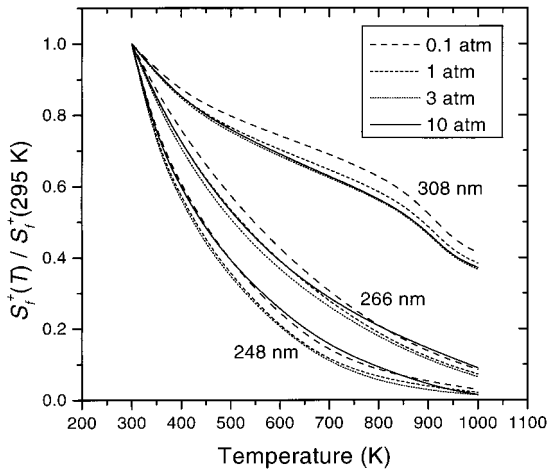

Fig. 14. Model-generated curves of fluorescence per unit mole fraction per unit laser fluence, plotted for three wavelengths and four different pressures. Each curve is normalized to unity at room temperature.

D. Dual-Wavelength Temperature Imaging

Model-generated fluorescence ratio curves that facilitate application of dual-wavelength temperature diagnostics at four selected pressures are given in Fig. 16. The slopes of the ratio curves for the respective pressures can be markedly different, especially for the 308–248-nm wavelength pair at high temperatures, suggesting that it is important to apply the appropriate curve for an experiment at a given uniform pressure. Dual-wavelength temperature sensitivity is typically slightly poorer than single-wavelength sensitivity. Random temperature uncertainties are shown in Fig. 17 for constant acetone partial pressure and total pressures from 0.5 to 5 atm, plotted in increments of 0.5 atm. Both 308–248-nm and 308–266-nm wavelength pairs have the lowest percentage temper-

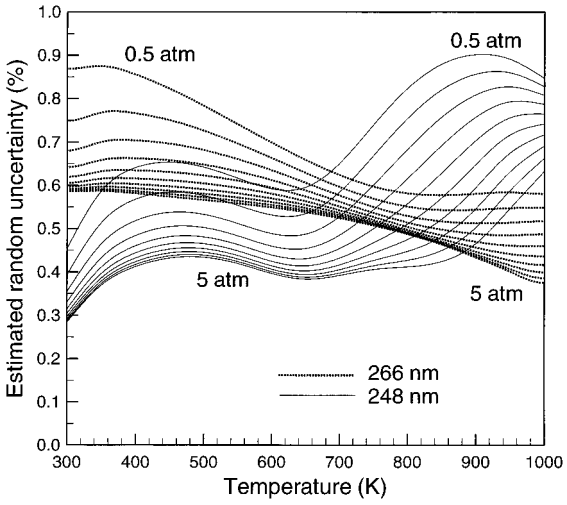

Fig. 15. Estimated single-wavelength temperature uncertainties for a hypothetical, shot-noise-limited experiment (see text). Families of curves, with pressure varying from 0.5 to 5 atm in 0.5-atm increments, are plotted for 248- and 266-nm excitation.

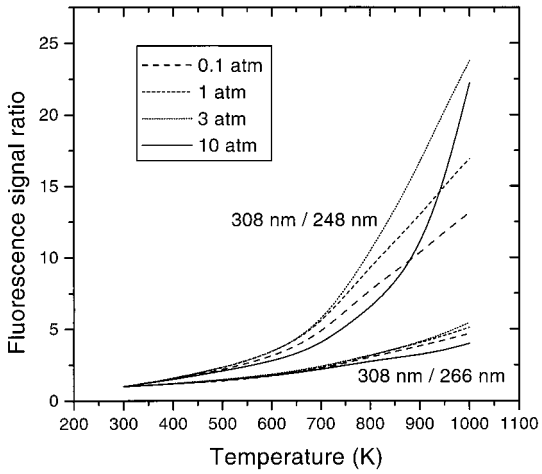

Fig. 16. Normalized, model-generated fluorescence ratio curves (as in Fig. 8), plotted for two wavelength pairs and four different pressures.

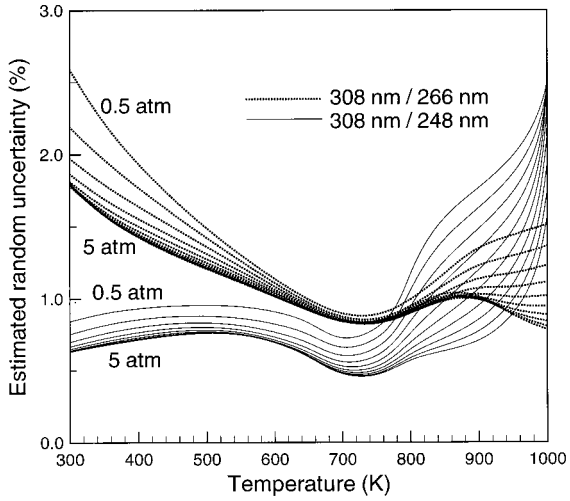

Fig. 17. Dual-wavelength temperature uncertainties plotted for hypothetical, shot-noise-limited experimental conditions (see text), with constant acetone partial pressure. Families of curves, with pressure varying from 0.5 to 5 atm in 0.5-atm increments, are plotted for the 308–248-nm and 308–266-nm wavelength pairs.

ature uncertainty near 700 K. As with the single-wavelength approach, sensitivity improves with increasing pressure.

If they are not accounted for, variations in pressure across a flow field will lead to errors in the temperature measured with dual-wavelength acetone PLIF. Figure 18 facilitates an assessment of this effect, plotting dT/dP, the error in measured temperature associated with a differential change in pressure. As in Fig. 17, curves are plotted for a range of pressures (again, in 0.5-atm increments). A clear conclusion from Fig. 18 is that pressure variation can cause significant errors in temperature, especially near room temperature. For example, at 300 K and 1 atm, for the 308–266-nm strategy, a pressure increase of only 0.1 atm across the flow will lead to a roughly 8-K temperature error. Errors for the 308–248-nm line pair are typically slightly less. Even though the effect of pressure on the fluorescence signal ratio makes the dual-wavelength technique less useful for measurements in flows with both pressure and acetone mole fraction variations, the dual-wavelength approach retains the advantage over single-wavelength measurements that temperature can be measured where seeding is variable.

E. Effects of Composition

Qualitative understanding of possible composition dependences on fluorescence quantum yield can be important for diagnostic applications. As in the case of pressure, composition that is uniform but different from that of the mixture for which the fluorescence data were obtained (acetone dilute in nitrogen) can in theory be corrected for by appropriate alteration of the value of $k_{coll}\alpha$ in the model and generation of new fluorescence–temperature curves. Unfortunately, this is often difficult in practice because of the uncertainty in unknown α for vibrationally excited acetone in the presence of different bath gases. If pressure-dependent fluorescence data are available for the mixture of interest, the $k_{coll}\alpha$ product can be set empirically, as was done in this study for nitrogen.

Lacking empirical calibration, one can use published data[35,39–41] on collisional energy transfer for other vibrationally excited polyatomic molecules to draw broad conclusions about the importance of compositional effects. In particular, studies[39–41] have suggested that energy transferred per collision ΔE_{coll}, and therefore α, is roughly correlated with number of atoms in the collider molecule. Collision rate k_{coll} is approximately proportional to the reciprocal of the square root of the reduced mass of the excited molecule with its collisional partner. Consideration of these two effects suggests that there will be little

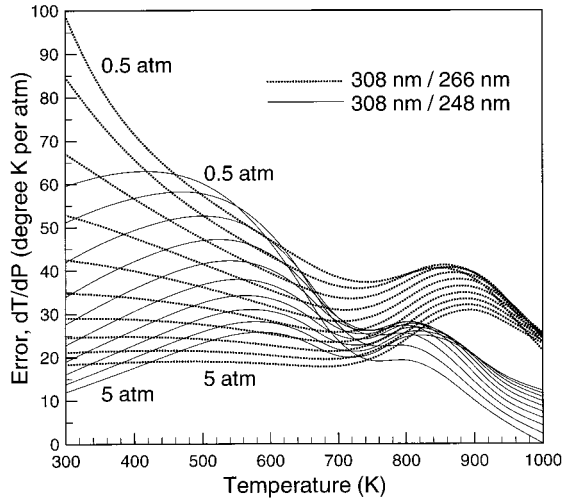

Fig. 18. Error in measured temperature with the dual-wavelength strategy that is due to a differential change in pressure. Families of curves, with pressure varying from 0.5 to 5 atm in 0.5-atm increments, are plotted for the 308–248-nm and 308–266-nm wavelength pairs.

difference in $k_{coll}\alpha$ between dilute acetone–nitrogen mixtures and dilute acetone–air mixtures. Consistent with this supposition, Ossler and Aldén[13] found no detectable difference in acetone fluorescence lifetime with nitrogen and air bath gases at 1 atm.

Even in mixtures of significantly different $k_{coll}\alpha$, errors owing to the use of the nitrogen fluorescence–temperature curves for diagnostic applications may remain small, both because of the indirect nature of the composition effect and because these curves incorporate fluorescence quantum yield on a relative basis only. Collisional parameters can be estimated in a rough way by analogy to the results of Hippler *et al.*[35] for azulene, another large organic molecule. For example, one can compare acetone in a helium bath gas with acetone in a nitrogen bath gas. For azulene, α is estimated[35] to be 0.017 for nitrogen collisions and 0.006 for helium collisions; we assume that this approximate factor-of-3 difference is also observed in the acetone system. The acetone–nitrogen collision rate is approximately two times lower than the acetone–helium collision rate. Taking these effects together, one estimates the vibrational energy decay rate of acetone in helium to be approximately two thirds that of acetone in nitrogen. Analysis with the model suggests that this change in vibrational relaxation rate will cause temperature results obtained with the acetone–nitrogen fluorescence data to be in error by not more than 5% for both single- and dual-wavelength strategies.

Cases with unknown and significantly variable composition across the flow require somewhat more attention to temperature errors. In such cases, variation in fluorescence owing to composition change can be indistinguishable from variation in fluorescence owing to temperature change. This temperature error is analogous to that from pressure variation (Fig. 18); both result from changes in $k_{coll}\alpha$ across the flow field. Therefore one can use Fig. 18 to conclude that, at 1 atm and 300 K, a 30% change in $k_{coll}\alpha$ owing to composition variation (equivalent to a pressure change of 0.3 atm) across the flow will result in roughly 25-K error for the 308–266-nm approach and 15-K error for the 308–248 nm approach.

Effects of variable composition across a flow field could potentially become significant in flows with high, variable (e.g., 0–20%) acetone seeding. Assuming that energy transfer efficiency roughly tracks molecular size, vibrational relaxation of acetone by acetone might be appreciably faster than that by nitrogen or oxygen. As a result, fluorescence yield might be expected to change enough between regions of maximum and minimum seeding to cause errors in highly quantitative applications. Preliminary experiments by Lozano[17] with 308-nm excitation did not reveal a significant effect of acetone mole fraction at atmospheric pressure and seedings of 4–12%; however, further study at this and other wavelengths is needed.

An evident composition effect that is not predicted by the model is quenching of fluorescence owing to oxygen at high pressure. This effect, observed in several studies,[9,12,13] seems to be highly nonlinear with pressure, becoming significant only above 3–5 atm. The triplet character of oxygen makes oxygen-enhanced intersystem crossing[42] a possible explanation for this phenomenon. Although experimental and theoretical data on this effect are too sparse to be incorporated into the model at present, further experiments to elucidate such behavior would be useful from a diagnostic point of view because many flows of interest include oxygen at higher pressure. For the moment, the important conclusion to be drawn is that oxygen does not appear to have a significant effect below ~3 atm but may start to quench fluorescence at higher pressures, most likely through a non-Stern–Vollmer-type effect on the intersystem crossing rate.

F. Multiparameter Imaging Approaches

Improved understanding of acetone photophysics based on experimental and modeling results permits the development of multiparameter imaging diagnostics that simultaneously measure temperature and one other quantity. Preliminary multiparameter imaging results have been obtained and will be reported in detail separately; the purpose of the discussion herein is to introduce and evaluate several possible multiparameter strategies in light of the photophysics results. For the moment, we limit consideration to dual-wavelength approaches.

Using an interline transfer CCD camera and two excimer lasers, at 308 and 248 nm (or, alternatively, replacing the 248-nm excimer with a frequency-quadrupled Nd:YAG at 266 nm), one can apply an instantaneous, dual-wavelength measurement technique with only a moderate increase in experimental complexity from that of the single-wavelength approach. Interline transfer CCD cameras developed in the past few years (e.g., Kodak Megaplus ES1.0 and Princeton Instruments CCD-1360SO) are capable of recording fluorescence images separated in time by as little as 1 μs, shorter than flow time scales in most cases. Assuming this kind of near-simultaneous imaging capability, we evaluate the following applications: (1) imaging of temperature and mixture fraction in flows with T, P, and acetone mole fraction χ varying, (2) imaging of temperature and mixture fraction with uniform P, and (3) imaging of temperature and pressure with uniform χ.

1. *Variable* T, P, *and* χ

Because of the pressure-related errors in the measured temperature, imaging of temperature and mole fraction with a dual-wavelength technique will be possible only under restricted conditions in this situation. For example, for a flow near atmospheric pressure with temperatures near 900 K, and only limited (say, 0.5-atm) pressure variation, the error in measured temperature that is due to pressure variation for a 308–248-nm ratio might be acceptably small (5 or 6 K), with random uncertainties near 1.7% (~15 K). Alternatively, a higher-pressure (~5-atm) 308–248 nm experiment at 300 K would also be expected to have a temperature error of only approxi-

mately 5 or 6 K because of a 0.5-atm pressure fluctuation, with an estimated random uncertainty near 0.6% (2 K). For many cases, however, temperature errors that are due to pressure fluctuations can be unacceptably large. In the future, triple-excitation-wavelength methods could possibly be used to image T, P, and χ, simultaneously.

2. *Uniform* P *and Variable* T *and* χ

Imaging temperature and mole fraction under conditions of uniform pressure is both feasible and of practical interest. The ratio of fluorescence images can be converted to a map of temperature by use of the model-generated curve for the pressure in question. The mixture fraction is then obtained by use of the less temperature-sensitive of the two fluorescence images (that from 308-nm excitation, for example), with correction for the known temperature variation across the flow field.

One could envisage an application that maps fuel–air mixture fraction and temperature inside an optically accessible engine cylinder at a specific instant in the compression cycle before combustion. A uniform pressure of several atmospheres might be expected in this case, with a temperature variation from 300 to 800 K. Acetone seeded into the fuel would permit measurement of mixing. Highly quantitative experiments might require characterization of and correction for the possible effects on fluorescence yield of the variable air–fuel mixture across the flow field. Another application of dual-wavelength acetone PLIF could involve gas-phase measurement of temperature and mixture fraction in evaporating sprays.

3. *Uniform* χ *and Variable* T *and* P

With constant seeding it is possible to image both T and P simultaneously. The ratio of fluorescence images, although it remains a function of pressure through the fluorescence-yield ratio, gives an initial estimate of temperature. The 308-nm image, corrected for this temperature variation, can then be used as a sensitive indication of pressure, because the single-wavelength signal at constant χ is a stronger than the linear function of P. An accurate final solution for both T and P can be obtained by iteration or solution of two equations in two unknowns at each point in the image. Simultaneous measurement of T and P could be useful for flow configurations that are amenable to constant acetone seeding: environments characterized by turbulent heat transfer, for instance, or supersonic flows with expansions and weak shocks, as in an underexpanded, free jet.

5. Conclusions

Fundamental studies of the variation of acetone fluorescence with excitation wavelength, temperature, pressure, and composition have established a body of data that can be applied to development of quantitative imaging diagnostics for acetone-seeded gaseous flows. Early single- and dual-wavelength imaging results that were described separately[11] have been based on the experimental measurements of the temperature dependence of acetone fluorescence presented here. Although imaging applications to date have been limited to 1 atm, the photophysics modeling described here has permitted the potential for temperature and multiparameter diagnostics to be investigated over a much wider range of conditions. Further photophysical investigations, in particular to verify pressure effects, to explore bath-gas dependences more quantitatively, and to reproduce the reported fluorescence quenching effect of oxygen at high pressures, would help to corroborate the model results and extend still further the regime of diagnostic applicability. For example, the model prediction of a fluorescence-yield high-pressure limit for a given temperature, if supported by experiment, might allow diagnostics to be applied above a certain pressure with less concern for effects of pressure and composition on fluorescence yield. Additional experimental studies of acetone photophysics would be usefully complemented by further modeling efforts, perhaps ones that treat distributions and collisions more realistically by use of the detailed "master equation"[43] formulation.

This research was sponsored by the U.S. Air Force Office of Scientific Research, Aerospace and Materials Sciences Directorate, with Julian Tishkoff as the technical monitor. Frédéric Grisch was supported by the Office National d'Études et de Recherches Aérospatiales and by the Direction de la Recherche et des Études Techniques, French Ministry of Defense. Martin Votsmeier was supported by the Deutsche Forschungsgesellschaft.

References

1. A. Lozano, B. Yip, and R. K. Hanson, "Acetone: a tracer for concentration measurements in gaseous flows by planar laser-induced fluorescence," Exp. Fluids **13,** 369–376 (1992).
2. A. Lozano, S. H. Smith, M. G. Mungal, and R. K. Hanson, "Concentration measurements in a transverse jet by planar laser-induced fluorescence of acetone," AIAA J. **32,** 218–221 (1993).
3. B. Yip, M. F. Miller, A. Lozano, and R. K. Hanson, "A combined OH/acetone planar laser-induced fluorescence imaging technique for visualized combusting flows," Exp. Fluids **17,** 330–336 (1994).
4. N. P. Tait and D. A. Greenhalgh, "2D laser induced fluorescence imaging of parent fuel fraction in nonpremixed combustion," in *Twenty-Fourth Symposium* (*International*) *on Combustion, Sydney, Australia* (Combustion Institute, Pittsburgh, Pa., 1992) pp. 1621–1628.
5. N. T. Clemens and P. H. Paul, "Effects of heat release on the near field flow structure of hydrogen jet diffusion flames," Combust. Flame **102,** 271–284 (1995).
6. D. Wolff, H. Schluter, V. Beushausen, and P. Andresen, "Quantitative determination of fuel air mixture distributions in an internal combustion engine using PLIF of acetone," Ber. Bunsenges. Phys. Chem. **97,** 1738–1741 (1993).
7. S. H. Smith and M. G. Mungal, "Mixing, structure and scaling of the jet in crossflow," J. Fluid Mech. **357,** 83–122 (1998).
8. J. B. Ghandhi and P. G. Felton, "On the fluorescence behavior of ketones at high temperatures," Exp. Fluids **21,** 143–144 (1996).
9. F. Grossmann, P. B. Monkhouse, M. Ridder, V. Sick, and J. Wolfrum, "Temperature and pressure dependences of the

laser-induced fluorescence of gas-phase acetone and 3-pentanone," Appl. Phys. B **62,** 249–253 (1996).
10. F. Grisch, M. C. Thurber, and R. K. Hanson, "Mesure de température par fluorescence induite par laser sur la molécule d'acétone," Rev. Sci. Tech. Defense **4,** 51–60 (1997).
11. M. C. Thurber, F. Grisch, and R. K. Hanson, "Temperature imaging with single- and dual-wavelength acetone planar laser-induced fluorescence," Opt. Lett. **22,** 251–253 (1997).
12. L. S. Yuen, J. E. Peters, and R. P. Lucht, "Pressure dependence of laser-induced fluorescence from acetone," Appl. Opt. **36,** 3271–3277 (1997).
13. F. Ossler and M. Aldén, "Measurements of picosecond laser induced fluorescence from gas phase 3-pentanone and acetone: implications to combustion diagnostics," Appl. Phys. B **64,** 493–502 (1997).
14. A. J. Hynes, E. A. Kenyon, A. J. Pounds, and P. H. Wine, "Temperature dependent absorption cross-sections for acetone and *n*-butanone—implications for atmospheric lifetimes," Spectrochim. Acta A **48,** 1235–1242 (1992).
15. M. Baba and I. Hanazaki, "The S_1, $^1A_2(n, \pi^*)$ state of the acetone in a supersonic nozzle beam: methyl internal rotation," Chem. Phys. Lett. **103,** 93–97 (1983).
16. H. Zuckermann, Y. Haas, M. Drabbels, J. Heinze, W. L. Meerts, J. Reuss, and J. v. Bladel, "Acetone, a laser-induced fluorescence study with rotational resolution at 320 nm," Chem. Phys. **163,** 193–208 (1992).
17. A. Lozano, "Laser-excited luminescent tracers for planar concentration measurements in gaseous jets," Ph.D. dissertation (Stanford University, Stanford, Calif., 1992).
18. D. A. Hansen and E. K. C. Lee, "Radiative and nonradiative transitions in the first excited singlet state of symmetrical methyl-substituted acetones," J. Chem. Phys. **62,** 183–189 (1975).
19. G. D. Greenblatt, S. Ruhman, and Y. Haas, "Fluorescence decay kinetics of acetone vapor at low pressures," Chem. Phys. Lett. **112,** 200–206 (1984).
20. R. A. Copeland and D. R. Crosley, "Radiative, collisional and dissociative processes in triplet acetone," Chem. Phys. Lett. **115,** 362–368 (1985).
21. A. Costela, M. T. Crespo, and J. M. Figuera, "Laser photolysis of acetone at 308 nm," J. Photochem. **34,** 165–173 (1986).
22. M. J. G. Borge, J. M. Figuera, and J. Luque, "Study of the emission of the excited acetone vapour at intermediate pressures," Spectrochim. Acta A **46,** 617–621 (1990).
23. J. Heicklen, "The fluorescence and phosphorescence of biacetyl vapor and acetone vapor," J. Am. Chem. Soc. **81,** 3863–3866 (1958).
24. A. M. Halpern and W. R. Ware, "Excited singlet state radiative and nonradiative transition probabilities for acetone, acetone-d_6, and hexafluoreacetone in the gas phase, in solution, and in the neat liquid," J. Chem. Phys. **54,** 1271–1276 (1971).
25. J. Ernst, K. Spindler, and H. G. Wagner, "Untersuchungen zum thermischen Zerfall von Acetaldehyd und Aceton," Ber. Bunsenges. Phys. Chem. **80,** 645–650 (1976).
26. J. C. Hsieh and E. C. Lim, "Internal conversion in isolated aromatic molecules," J. Chem. Phys. **61,** 736–737 (1974).
27. K. F. Freed, "Collisional effects on electronic relaxation processes," in *Potential Energy Surfaces*, K. P. Lawley, ed. (Wiley, New York, 1980), pp. 207–269.
28. R. G. Shortridge, Jr., C. F. Rusbult, and E. K. C. Lee, "Fluorescence excitation study of cyclobutanone, cyclopentanone, and cyclohexanone in the gas phase," J. Am. Chem. Soc. **93,** 1863–1867 (1970).
29. D. J. Wilson, B. Noble, and B. Lee, "Pressure dependence of fluorescence spectra," J. Chem. Phys. **34,** 1392–1396 (1961).
30. G. B. Porter and B. T. Connelly, "Kinetics of excited molecules. II. Dissociation processes," J. Chem. Phys. **33,** 81–85 (1960).
31. G. H. Kohlmaier and B. S. Rabinovitch, "Collisional transition probabilities for vibrational deactivation of chemically actived *sec*-butyl radicals. The rare gases," J. Chem. Phys. **38,** 1692–1714 (1963).
32. A. N. Strachan, R. K. Boyd, and K. O. Kutschke, "Multistage deactivation in the photolysis of hexafluoroacetone," Can. J. Chem. **42,** 1345–1354 (1963).
33. J. Troe, "Approximate expressions for the yields of unimolecular reactions with chemical and photochemical activation," J. Phys. Chem. **87,** 1800–1804 (1983).
34. E. K. C. Lee and R. S. Lewis, "Photochemistry of simple aldehydes and ketones in the gas phase," Adv. Photochem. **12,** 1–95 (1980).
35. H. Hippler, B. Otto, and J. Troe, "Collisional energy transfer of vibrationally highly excited molecules. IV. Energy dependence of $\langle \Delta E \rangle$ in azulene," Ber. Bunsenges. Phys. Chem. **93,** 428–434 (1989).
36. T. Shimanouchi, *Tables of Molecular Vibrational Frequencies, Consolidated Volume I*, Natl. Stand. Ref. Data Ser. Natl. Bur. Stand. **39,** (1972).
37. R. B. Cundall and A. S. Davies, "The mechanism of the gas phase photolysis of acetone," Proc. Soc. London Ser. A **290,** 563–582 (1966).
38. G. M. Breuer and E. K. C. Lee, "Fluorescence decay times of cyclic ketones, acetone, and butanal in the gas phase," J. Phys. Chem. **75,** 989–990 (1970).
39. M. J. Rossi, J. R. Pladziewicz, and J. R. Barker, "Energy-dependent energy transfer: deactivation of azulene (S_0, E_{vib}) by 17 collider gases," J. Chem. Phys. **78,** 6695–6708 (1983).
40. H. Hippler, J. Troe, and H. J. Wendelken, "Collision deactivation of vibrationally highly excited polyatomic molecules. II. Direct observations for excited toluene," J. Chem. Phys. **78,** 6709–6717 (1983).
41. H. Hippler, J. Troe, and H. J. Wendelken, "Collisional deactivation of vibrationally highly excited polyatomic molecules. III. Direct observations for substituted cycloheptatrienes," J. Chem. Phys. **78,** 6718–6724 (1983).
42. W. M. Nau and J. C. Scaiano, "Oxygen quenching of excited aliphatic ketones and diketones," J. Phys. Chem. **100,** 11,360–11,367 (1996).
43. J. Troe, "Collisional deactivation of vibrationally highly excited polyatomic molecules. I. Theoretical analysis," J. Chem. Phys. **77,** 3485–3492 (1982).